Ann. Phys. (Berlin) **528**, No. 5, 365–372 (2016) / DOI 10.1002/andp.201500348

annalen der physik

Phonon-polariton entrapment in homogenous surface phonon cavities

Didit Yudistira[1,2,*], *Andreas Boes*[1,2], *Benjamin Dumas*[1,2], *Amgad R. Rezk*[4], *Morteza Yousefi*[3], *Bahram Djafari-Rouhani*[5], *Leslie Y. Yeo*[4], *and Arnan Mitchell*[1,2]

Received 1 December 2015, revised 11 January 2016, accepted 12 January 2016
Published online 8 February 2016

Surface phonon cavities that are homogenous in both mechanical and dielectric properties are reported. The cavities are formed by the placement of a defect of a single domain within periodic domain inversion of single crystal piezoelectric lithium niobate that exhibits surface phononic bandgap through the phonon-polariton coupling. Surface cavity resonances are observed within the bandgap, which manifest in entrapment of phonon-polariton within the defect. In addition to demonstrating that the observed resonances are non-radiative and decoupled to bulk radiation, which is critical for high Q cavities, it is also shown the possibility to tune the surface cavity resonance spectra simply by varying the defect width. Such an ability to excite surface cavity resonance that is non-radiative with simultaneous localization of the electric field together with the advantage of a cavity that is physically formed from a completely monolithic and uniform material offers unique opportunities for widespread applications for example in actuation, detection, and phonon lasing that can be fully integrated with other physical systems such as quantum acoustics, photonics, and microfluidics.

Phononic bandgap structures and phononic crystals are novel class of materials, which have emerged as promising candidates to control the suppression and redirection of phonon propagation in controlled manner in contrast to their behavior in unstructured bulk materials, given rise by their unique properties, namely phononic bandgaps [1–3] and negative refraction [4]. The ability for such control is crucial for current research in phonon-mediated photonic interactions [5–9], quantum physics [10–13], biosensing [14, 15], and nano-scale thermal management [16, 17]. A critical requirement in many of these applications is the ability to insulate a region of interest from random phonons in the environment. Reports have shown that if a defect is embedded within a phononic bandgap structure, a phonon cavity can be formed [18–22], enabling the trapping and concentration of phonons of a specific resonant frequency in a desired location, which has been observed via a picosecond ultrasonic technique [21], by Brillouin light scattering [19] or Raman spectra [18]. Dynamic tuning of these phonon cavity resonances can be directly achieved by controlling defect parameters, thus facilitating a number of applications, such as acoustic diodes [23], coherent phonon generation [20–22], thermal control [16, 17], and concurrent phonon-photon modulation [24, 25].

The vast majority of the research [18–22], nevertheless, have been carried out to obtain phononic cavities for *bulk* waves; these structures typically comprising periodic composite media, often exclusively engineered from multi-layer single crystal semiconductor materials, achieved by molecular beam epitaxy. On the other hand, cavities for *surface* acoustic waves (SAWs) are highly desirable due to the enhanced concentration of acoustic energy at the surface that can facilitate direct coupling with other physical systems [5, 14]. In the context of piezoelectric materials, the electric fields that accompany the SAW propagation have recently been shown to play an important role in enabling the observation of

* Corresponding author: E-mail: didit.yudistira@rmit.edu.au
[1] School of Electrical and Computer Engineering, RMIT University, Melbourne, VIC 3001, Australia
[2] ARC Centre of Excellence for Ultrahigh Bandwidth Devices and Optical Systems, RMIT University, VIC 3001, Melbourne, Australia
[3] School of Aerospace, Mechanical and Manufacturing Engineering, RMIT University, VIC 3001, Melbourne, Australia
[4] Micro/Nanophysics Research Laboratory, RMIT University, Melbourne, VIC 3001, Australia
[5] Institut d'Electronique, de Micréoelectronique et de Nanotechnologie (IEMN), UMR CNRS 8520, Université de Lille 1, 59655 Villeneuve d'Ascq Cedex, France

coherent single-electron dynamics [26], and control of electron-hole pair in low dimensional structure, such as graphene [27–29]. To date, however, a surface phononic bandgap structure —the building block to forming a surface cavity—has either been formed from an array of holes or pillars, or layers of different materials at the surface of the host substrate matrix [3, 30]. This additional layer on the substrate surface can present a barrier for integration with other physical systems, such as optical waveguides to realize an opto-mechanical system [8], microchannels for microfluidic applications [14], or graphene [27–29]. Moreover, while piezoelectric surface phononic bandgap structures have been demonstrated, [31–33] there has yet to be a report showing the possibility of controlling the propagation of the accompanying electric fields.

In previous recent work, we have demonstrated that surface phononic bandgap can be achieved in a material that is mechanically, electromechanically, and topographically homogeneous, without any physical alteration of the surface, but simply formed by periodically reversing the sign of the piezoelectric tensor e in single crystal lithium niobate [34, 35], in contrast to past approaches with holes and pillars [3, 30]. The bandgap is exhibited through phonon-polariton coupling, yielding the simultaneous suppression of the propagation of both the surface phonons and the accompanying electric field in a specific frequency range, determined by the structure period a. Unlike phonon-polariton usually observed in nano-sized polar materials that involves optical phonons operating in the mid-IR to THz spectral ranges [36], the phonon-polariton considered here is mainly related to the interaction between electromagnetic waves and acoustic phonons, which occur in much lower frequency. Both one-dimensional (1D) [37] and two-dimensional (2D)[38] phonon-polariton bandgap structures were demonstrated and analyzed. In particular, the integration into a linear integrated optical [39–41] and microfluidic systems [42] have been also shown in the 1D structure, demonstrating that these monolithic bandgap structures represent a highly integrable phononic platform.

In this report, we introduce a surface phonon cavity achieved by placement of a defect of a single domain within a one-dimensional periodic domain inversion of a single crystal piezoelectric lithium niobate. The structure is homogeneous in both mechanical and dielectric properties, requiring no machining or deposition of materials and without the need to adjust the mass or stiffness. We demonstrate that the proposed cavity can exhibit entrapment of phonon-polariton, indicated by the simultaneous spatial localization of both the surface phonons and the electric fields within the defect. To our best knowledge, this is the first report showing the formation of a surface phonon-polariton cavity, and is further distinguished from previous work by its demonstration on a homogenous material.

An illustration of the structure and a micrograph of the fabricated structure are shown in Figs. 1a and 1b, respectively. The cavity consists of a defect of unpoled material with a lateral width D placed at $x_c = A$ within a phonon-polariton bandgap structure as illustrated in Fig. 1a. A bandgap structure with a period $a = 20$ μm is considered, which corresponds to surface phononic bandgap at around 185 MHz as revealed by the calculated surface phononic band structure (see Fig. 2a) of an infinitely long periodic structure (displayed in the inset). The bandgap is indicated by the shaded area where an additional narrow bandgap at approximately 210 MHz above the surface phononic bandgap exists, likely corresponding to a radiative bandgap that can be attributed to a leaky SAW propagating at a velocity of 4400 m/s. To reveal the surface cavity resonance excitation as well as to gain insight into its resonant behavior, we calculate the frequency spectra of the amplitude response of the surface phonon displacement $|\mathbf{U}|$, which is determined on the defect area at $x_c = A$, while varying the defect width D from $0.5a$ to $1.0a$.

Figure 2b shows the contour of the calculated $|\mathbf{U}|$ in the frequency and defect width D space, revealing a distinct peak that traverses the bandgap as D varies from $0.5a$ to $1.0a$ or from 10 μm to 20 μm. As an example, we plot in Fig. 2c for three different defect widths, $D = 0.5a = 10$ μm, $0.75a = 15$ μm and $1.0a = 20$ μm, where we clearly observe distinct peaks located at the edges and within the bandgap, denoted by (i ii, vi), and (iii, iv, vi), respectively. Peaks iii, iv, and vi can thus be ascribed to surface cavity resonances, verified by the corresponding displacement plots in Fig. 2d. This cavity resonance originates from the surface phonons that are trapped by the defect and that oscillate back and forth within it while decaying outside the defect. As indicated by Fig. 2b, the frequency of the cavity resonance decreases as the D increases, because the trapped surface phonons have more space to oscillate. This may suggest that the frequency of the cavity resonance can be tuned through the modulation of the defect width D.

When $D = 0.5a$, the cavity resonance is not present in Fig. 2b as well as in the top panel of Fig. 2c, indicating that there are no surface phonons trapped within the defect as expected. Here, the structure behaves as a standard phononic bandgap for $D = 0$, which also corresponds to a non-defect cavity structure. We instead see two pronounced peaks located at the upper and

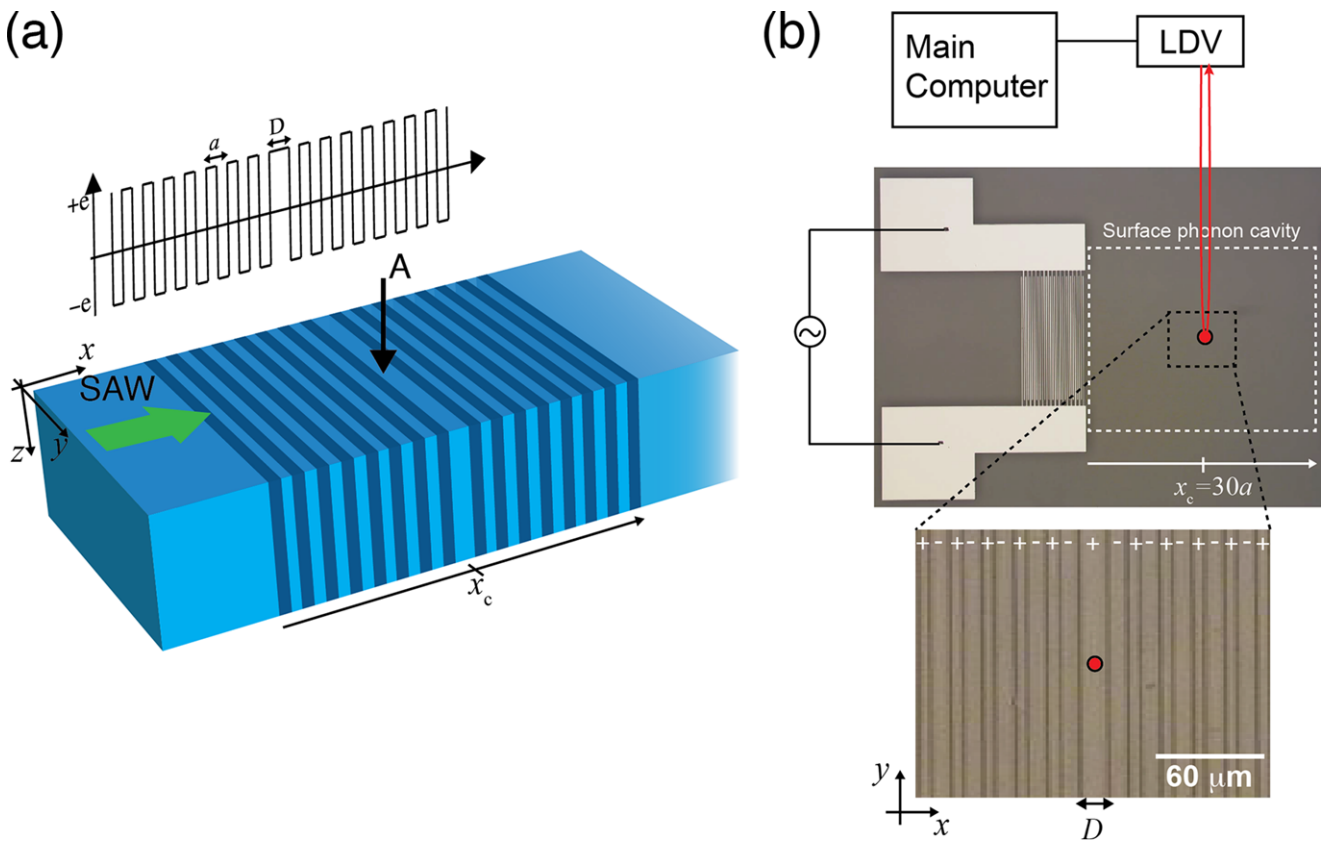

Figure 1 (a) Illustration of a surface phonon cavity with a bandgap structure consisting of regular poling with period a, and with an included defect of width D. The piezoelectric substrate has uniform mechanical and dielectric properties, but has either a positive or negative piezoelectric response e. The structure is probed with an incoming SAW (from the left) and the structure response is determined on the defect (the position of which is indicated by 'A'). (b) Microscope image of the fabricated surface phonon cavity and the IDTs used to generate the SAW. The region of the poled bandgap region is indicated by the larger white dashed rectangle and the region with the defect is indicated by the smaller dark dashed rectangle. Laser Doppler Vibrometry (LDV) visualization of the transmitted SAW is conducted on the far side of the defect as indicated by the spot on which the laser beam is focused. The cavity as measured is monolithic with no surface structure and is thus not evident in the image; the inset presents a magnified image of the region indicated by the dashed rectangle, taken after HF etching (post measurement) to reveal the domain structure forming the cavity.

lower edges of the bandgap denoted by peaks i, and ii, respectively, in the upper panel of Fig. 2c. These peaks can be associated with the edge resonance. Also, their corresponding displacement plots in the upper panel of Fig. 2d suggest that they are distributed with its maximum centered in the cavity. Given their group velocity is low, the surface phonons undergoes multiple reflections at the domain walls through a phonon-polariton coupling mechanism and therefore possess a long acoustical path. This may explain why their peaks are significantly larger compared to the others. When D is increased, the overall cavity length increases. As a result, the frequency of the upper edge resonance (peak i) monotonically decreases because the phonon has more space to propagate. At some point it approaches the cavity resonance at around $D = 0.75a$, resulting in the anticrossing of the dispersion curve [19]. As a consequence, two separate distinct peaks, iii and iv, are formed, as seen in the middle panel of Fig. 2c, corresponding to the cavity resonances as indicated by their displacement plots presented in the middle panel of Fig. 2d. Similarly, the lower edge resonance decreases as D increases and then merges with the lower frequency pass band. As expected, when the cavity is excited at a frequency gap, i.e., at vii in the lower panel of Fig. 2c for $D = 1.0a$, the surface phonons manifest as an evanescent wave within the cavity, caused by the phononic bandgap as expected.

To experimentally demonstrate the above results, four samples are prepared: unpoled lithium niobate

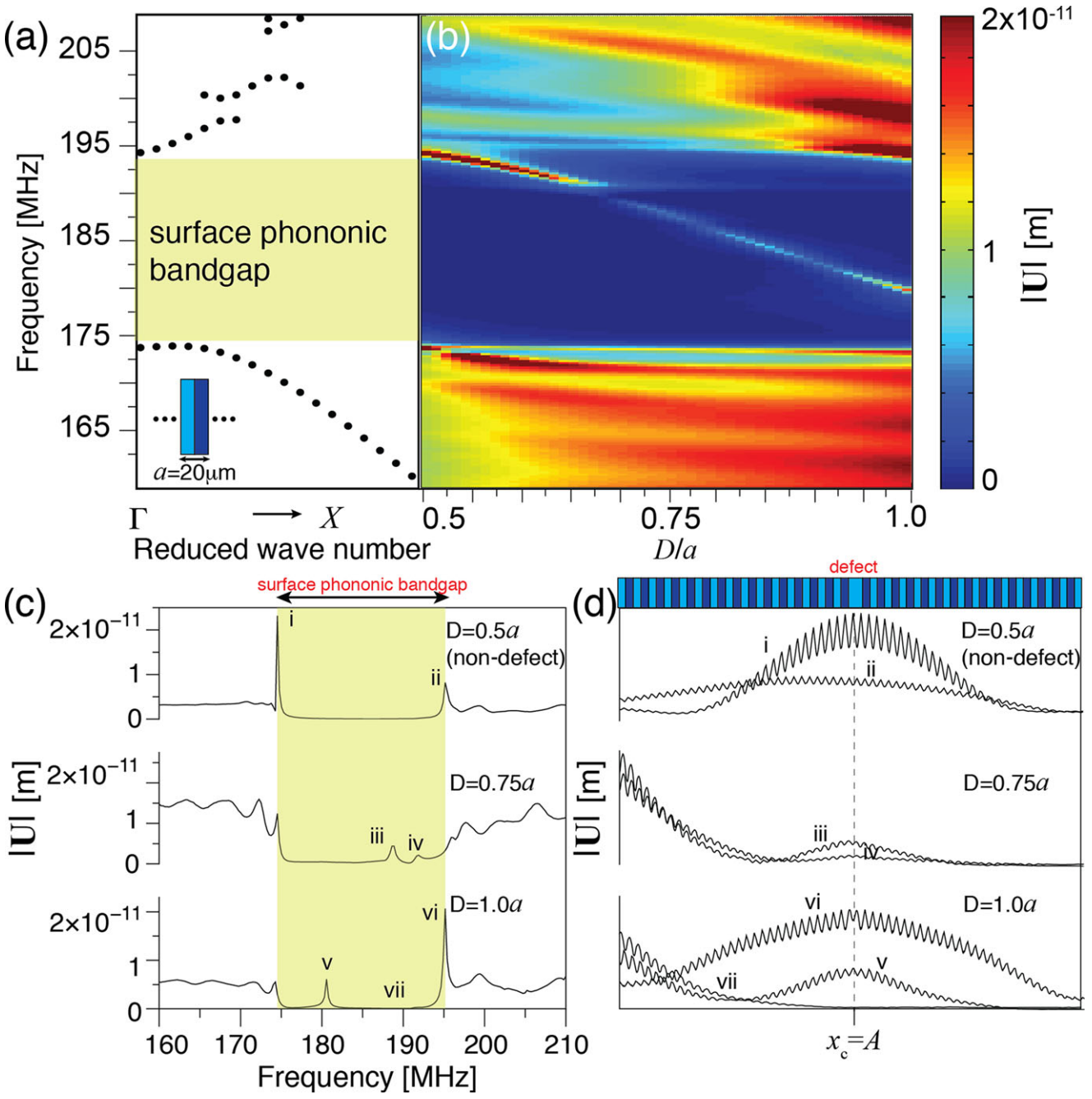

Figure 2 (a) Calculated surface phononic band structure for an infinite sequence of periodic domain inversions with period $a = 20\ \mu$m (unit cell shown in the inset). (b) Simulated map of the spectral response of the surface phonon displacement $|\mathbf{U}|$ as a function of the frequency and defect width D. (c) Simulated spectral responses of the surface phonon displacement $|\mathbf{U}|$ of the cavities with different defect widths; (top) non-defect structure ($D = 0.5a = 10\ \mu$m); (middle) cavity with width $D = 0.75a = 15\ \mu$m, and, (bottom) a cavity with width $D = 1.0a = 20\ \mu$m. (d) Corresponding displacement profiles within the cavity (illustrated by the inset), calculated at peaks (i, ii, vi) and (iii, iv and v), which corresponds to the edge and cavity resonances, respectively, for $D = 0.5a$ (top), $D = 0.75a$ (middle) and $D = 1.0a$ (bottom). Also plotted is the displacement calculated at vii, showing an evanescent wave characteristic associated with the bandgap.

(sample 1); a non-defect sample (or phononic bandgap structure) (sample 2) and two cavity samples with different defect widths, $D = 15$ μm (sample 3) and $D = 20$ μm (sample 4), respectively. Sample characterization is performed using a standard interdigital transducer (IDT) generating coherent SAW with a frequency that can be tuned between 175 – 195 MHz spanning the phononic bandgap in conjunction with the use of a laser Doppler vibrometer (LDV) to directly measure the surface phonon displacement $|\mathbf{U}|$ on the defect area. Fig. 1b shows the characterization setup used in our experiment.

The measured spectral responses of the surface phonon displacement $|\mathbf{U}|$ are presented in Figs. 3a–d for samples 1–4, respectively. Figure 3a presents the response from the blank sample, revealing the SAW bandwidth of the fabricated IDT. The ripple observed within the excitation band may be attributed to triple-transit signal [43]. Figure 3b shows the spectral response of the non-defect structure. Compared to the response observed from the blank sample in Fig. 3a, the surface displacement can be seen to be significantly reduced between 180 MHz and 190 MHz in Fig. 3b, clearly indicating the existence of a surface phononic bandgap as expected. The peaks at the upper and lower edges of the bandgap are evident in Fig. 3b, thus confirming the edge resonance as previously discussed. In particular, the existence of surface cavity resonances on cavity samples (samples 3 and 4) is well confirmed by the experiment, indicated by the peaks observed inside the bandgap as presented in Figs. 3c and 3d for $D = 0.75a = 15$ μm and $D = 1.0a = 20$ μm, respectively. In addition, we observe two peaks within the bandgap for $D = 0.75a$ in Fig. 3c that agrees well with the simulation, thus confirming the interaction between the upper edge and surface cavity resonances previously discussed. Overall experimental results presented in Figs. 3a–c appear to be in a good agreement with the simulation results in Fig. 2a. The small discrepancies between the experiment and the simulation possibly arise from the duty cycle of fabricated structures, which could have deviated slightly from 50%, which can further be confirmed by a magnified image of the cavity taken after HF etching (post measurement) in the inset of Fig. 1b.

To gain insights into the observed resonances, we excite the cavity of $D = 1.0a = 20$ μm at three different frequencies, corresponding to the peaks at v, and vi, and also at vii in the gap in Fig. 3d. For each frequency, we perform LDV area scans along the cavity parallel to the x axis to map the surface phonon displacement $|\mathbf{U}|$. The measured displacements $|\mathbf{U}|$ are presented in Figs. 4a–c for locations vii, v, and vi, respectively, in which the

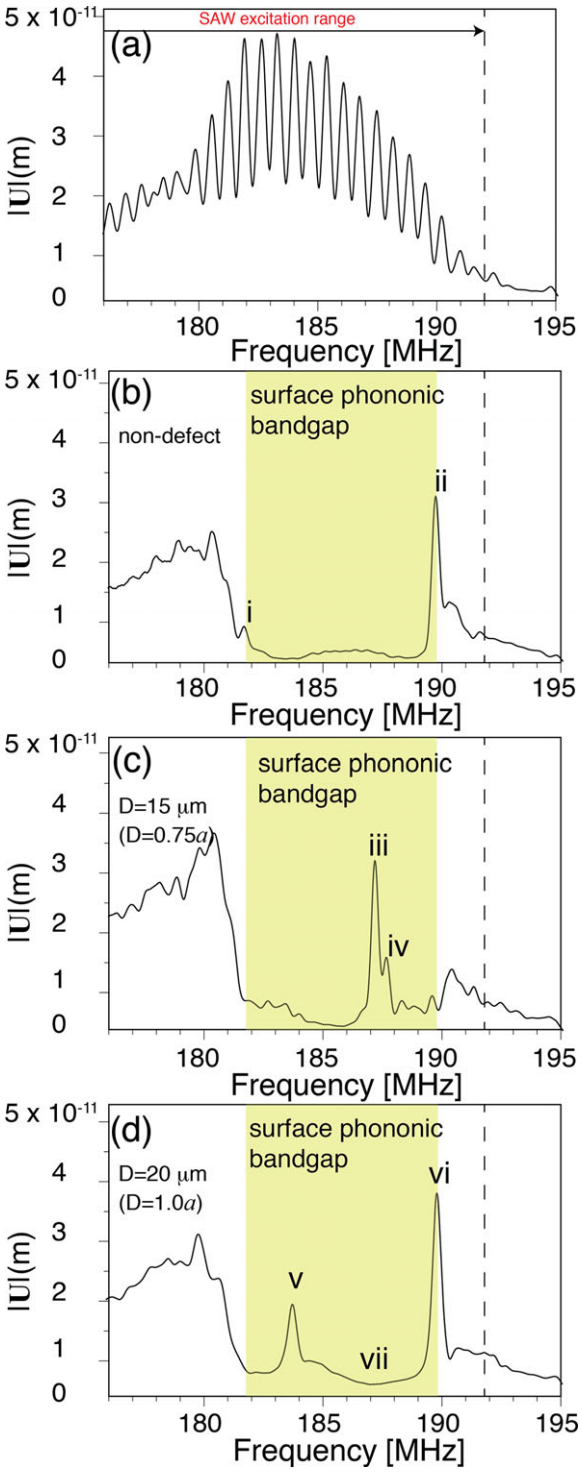

Figure 3 Measured spectral response of the surface displacement $|\mathbf{U}|$ obtained using the LDV from four different samples: (a) bare lithium niobate; (b) Phononic bandgap structure; and cavities that include a defect with (c) $D = 0.75a = 15$ μm, and (d) $D = 1.0a = 20$ μm. The lattice period a is 20 μm. The ripple within the SAW excitation range seen in (a) can be attributed to the triple-transit signal [43].

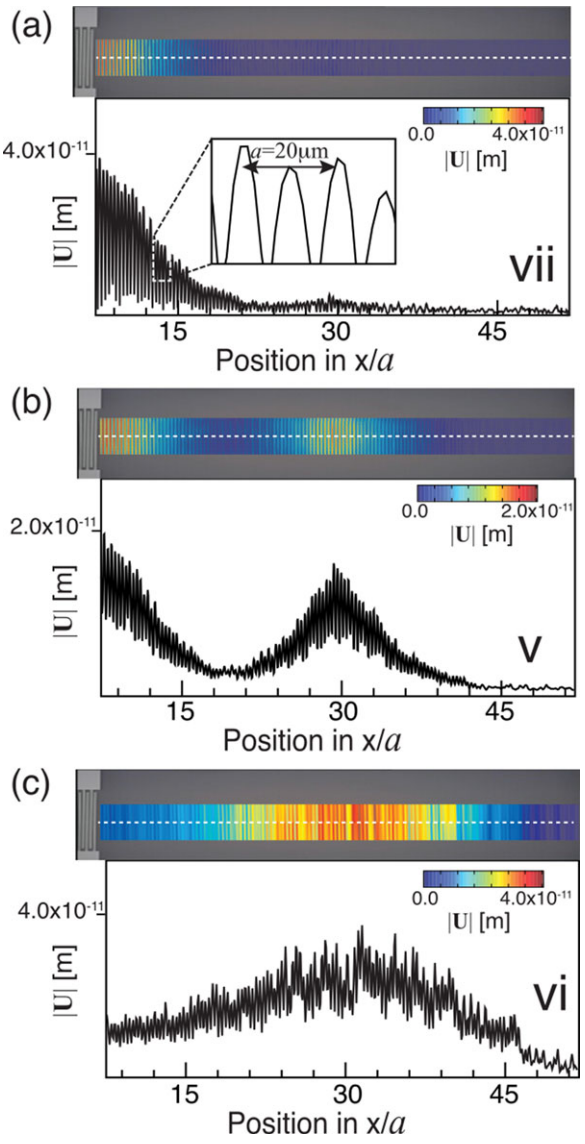

Figure 4 Maps of the displacement of surface phonons $|\mathbf{U}|$ in the x-y plane (upper panels) and along the white dashed line of the cavity (lower panels) measured using the LDV on a cavity with a defect of $D = 20$ μm at the three different locations, (a) inside the bandgap (vii), (b) at the cavity resonance (v), and, (c) at the edge resonance (vi), shown in Fig. 2d. The defect is located at approximately $x_c = 30a$.

upper panel displays the maps of the measured displacement $|\mathbf{U}|$ on x-y plane whereas the lower panel maps the displacement $|\mathbf{U}|$ along x-axis corresponding to the white dashed line. It is clear from Fig. 4a that the incident SAW is subjected to a strong reflection caused by surface phononic bandgap when the cavity is excited at a frequency within the bandgap. Moreover, the rapid oscillations observed in the measured values of $|\mathbf{U}|$ observed in Fig. 4a indicates a strong standing wave (corresponding to the periodicity of the bandgap structure shown in the inset) whose envelope attenuates approximately exponentially from the IDT into the cavity as expected for a phonon-polariton bandgap structure [37, 38]. When the cavity is excited at the cavity resonance, the surface phonons are trapped inside the defect, as shown by the localization of the surface displacement within this location in Fig. 4b, in good agreement with the calculation denoted by (v) in the lower panel of Fig. 2c, hence confirming the surface cavity resonance. At a frequency associated with the upper edge resonance, the surface phonon can indeed be seen to be bound within the cavity, following the prediction denoted by (vi) in the lower panel of Fig. 2c.

The LDV results in Fig. 4, nevertheless, comprise only measurements of the displacement amplitude $|\mathbf{U}|$ at the substrate surface. It would also be valuable to analyze the characteristics of the surface cavity resonance beneath the substrate of the cavity to qualitatively determine the quality of the resonance along with the accompanying electric fields $|\mathbf{E}|$ induced by the phonon-polariton coupling. As such, we plot in Fig. 5a the surface cavity displacement $|\mathbf{U}|$ across a cross-section along the y-z plane for a frequency associated with the cavity resonance (v) denoted in Fig. 2c corresponding to the cavity with $D = 1.0a$; other peaks inside the bandgap displays similar characteristics and are hence not shown. We also plot in the right panel of Fig. 5a the displacement $|\mathbf{U}|$ in the y-direction corresponding to a location along the white dashed-line, clearly showing the confinement of the displacement associated with the cavity resonance within a wavelength beneath the surface, evanescently extending into the substrate where coupling with the bulk radiation from the cavity is insignificant. These results suggest that the observed cavity resonance maintains its nature as a surface wave nature such that radiative losses are not a factor in the cavity's function, which can be a significant advantage when designing high Q resonators. Additionally, it can be seen from Fig. 5b that the accompanying electric field $|\mathbf{E}|$ is simultaneously localized within the defect area due to the phonon-polariton bandgap. Moreover, the field can also be observed to be confined strongly at the surface substrate, as confirmed by the plot in the right panel of Fig. 5b.

In summary, we have presented the first univocal observation of the entrapment of phonon-polariton in homogenous surface phonon cavities. The cavity is based on a phonon-polariton coupling within a bandgap structure that arises from periodic domain inversion on a single crystal piezoelectric lithium niobate with a defect

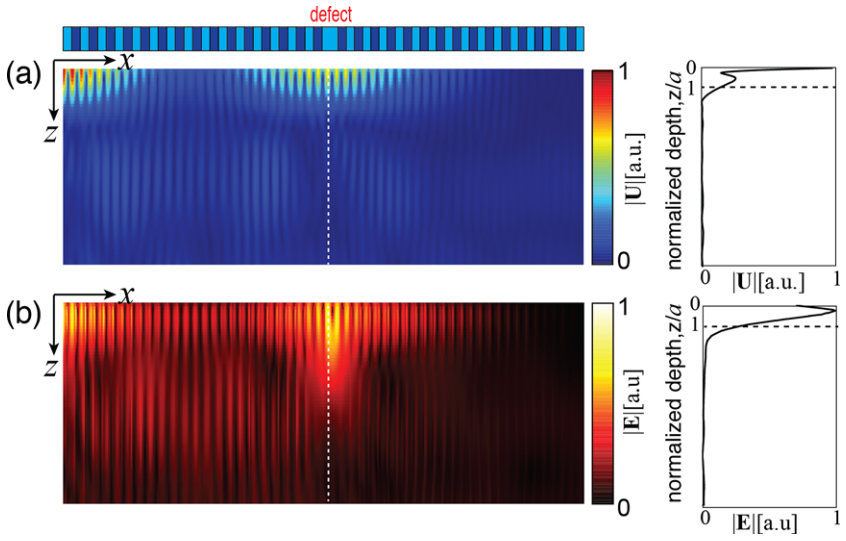

Figure 5 (a) Normalized calculated phononic displacement amplitude $|\mathbf{U}|$, and, (b) the accompanying electric field $|\mathbf{E}|$ passing through the cavity with $D = 1.0a$, corresponding to peak v in Fig. 2c, plotted in x-z plane. The images on the right are plots along the z-direction taken from the middle of the defect along the vertical white dashed line.

of a single domain. In addition to demonstrating that the observed resonances are non-radiative and decoupled to bulk radiation, which is critical for high Q cavities, we also show the possibility to tune the surface cavity resonance spectra simply by varying the defect width. Such an ability to excite surface cavity resonance that is non-radiative with simultaneous localization of the electric field together with the advantage of a cavity that is physically formed from a completely monolithic and uniform material offers unique opportunities for widespread applications for example in actuation, detection, and phonon lasing that can be fully integrated with other physical systems such as quantum acoustics, photonics, and microfluidics.

1 Experimental Section

1.1 Phonon cavity

The periodic domain inversion underlying the phonon cavity is fabricated through electric field poling on congruent Z-cut lithium niobate with a thickness of 500-μm, supplied by Gooch & Housego (Ilminster, UK). Prior to the poling process, an insulator based on AZ1512 photoresist is coated on the Z face and patterned using standard photolithography. The pattern consists of an array of stripes with width 13 μm widths and 1000 μm lengths, aligned along the x-direction. A large DC electric field that exceeds the coercive field for lithium niobate of 21.5 kV/cm is applied to the substrate through a contact with a liquid electrolyte consisting of LiCl in deionzed water. The spontaneous polarization of the crystal occurs locally on the exposed substrate. The chips are then treated in AZ100 solution to remove the photoresist.

1.2 Surface acoustic wave characterization

The SAW is generated by applying a RF signal to the IDT using a signal generator (Rhode & Schwarz, SML01, North Ryde, NSW, Australia) in conjunction with an amplifier (Mini Circuits ZHL-5W-1, 5–500 MHz, Brooklyn, NY, US) and 3 A, ±24 DC power supply. The IDT consists of 15 finger pairs of 5 μm width electrodes with a pitch of 20 μm and aperture of 650 μm fabricated on the Z face of lithium niobate through a lift-off process in acetone. Prior to lift-off, the IDT pattern is transferred on AZ1512 photoresist coated on the Z-cut lithium niobate substrate using standard photolithography followed by evaporative deposition of a 100 nm thick aluminum layer. The spectral response of the cavities along with maps of surface displacement reported in Figs. 3 and 4 respectively are then obtained using laser Doppler vibrometry (LDV; UHF-120, Polytec GmBH, Waldbronn, Germany).

1.3 Simulation

Numerical simulation is performed using COMSOL Multiphyisics v5.1 based on a finite element method. The surface phononic band structure associated with the phonon-polariton phononic crystal in Fig. 2a is computed by solving an eigenvalue problem in a 2D unit cell consisting of poled and unpoled regions, as shown in the inset of Fig. 2a, whose boundaries are prescribed with periodic boundary conditions. The thickness is set to 8 times the period a, and a perfectly matched layer (PML) boundary condition is prescribed along the bottom boundary. To identify the surface modes that represent the surface phononic band structure, mode

sorting is applied, considering only modes with 90% of its acoustic energy concentrated within one period a measured from the surface. The spectral responses of the cavity reported in Figs. 2b and 2c are computed based on a 2D model structure consisting of 30 periods with a 50% duty cycle between the poled and unpoled regions. A monochromatic SAW obtained from the solution of the IDT is then imposed in the cavity. In all simulations, the mechanical c and the electromagnetic ε tensors are held constant over the entire half-space occupied by the piezoelectric substrate, as is the magnitude of the piezoelectric coupling constant e, but the *signs* of the tensor are either positive or negative depending whether the location is within the unpoled and poled domain, respectively. The material properties of lithium niobate are taken from the material library provided in COMSOL.

Key words. phononic crystals, phononic bandgap, domain inversion lithium niobate, phonon polariton, surface acoustic wave.

References

[1] B. Djafari-Rouhani, A. A. Maradudin, and R. F. Wallis, Phys. Rev. B **29**, 6454 (1984).
[2] M. S. Kushwaha, P. Halevi, L. Dobrzynski, and B. Djafari-Rouhani, Phys. Rev. Lett. **71**, 2022 (1993).
[3] R. Olsson Iii and I. El-Kady, Meas. Sci. Technol. **20**, 012002 (2009).
[4] N. Fang, D. Xi, J. Xu, M. Ambati, W. Srituravanich, C. Sun, and X. Zhang, Nat. Mater. **5**, 452 (2006).
[5] R. Van Laer, B. Kuyken, D. Van Thourhout, and R. Baets, Nat Photon. **9**, 199 (2015).
[6] F. Brennecke, S. Ritter, T. Donner, and T. Esslinger, Science **322**, 235 (2008).
[7] B. J. Eggleton, C. G. Poulton, and R. Pant, Adv. Opt. Photonics **5**, 536 (2013).
[8] S. A. Tadesse and M. Li, Nat Commun **5** (2014).
[9] S. Kapfinger, T. Reichert, S. Lichtmannecker, K. Muller, J. J. Finley, A. Wixforth, M. Kaniber, and H. J. Krenner, Nat Commun **6** (2015).
[10] M. V. Gustafsson, T. Aref, A. F. Kockum, M. K. Ekström, G. Johansson, and P. Delsing, Science **346**, 207 (2014).
[11] A. D. O'Connell, M. Hofheinz, M. Ansmann, R. C. Bialczak, M. Lenander, E. Lucero, M. Neeley, D. Sank, H. Wang, M. Weides, J. Wenner, J. M. Martinis, and A. N. Cleland, Nature **464**, 697 (2010).
[12] S. Hermelin, S. Takada, M. Yamamoto, S. Tarucha, A. D. Wieck, L. Saminadayar, C. Bauerle, and T. Meunier, Nature **477**, 435 (2011).
[13] C. H. W. Barnes, J. M. Shilton, and A. M. Robinson, Phys. Rev. B **62**, 8410 (2000).
[14] J. Friend and L. Y. Yeo, Rev. Mod. Phys. **83**, 647 (2011).
[15] T. M. A. Gronewold, Anal. Chim. Acta. **603**, 119 (2007).
[16] M. Maldovan, Nature **503**, 209 (2013).
[17] M. Maldovan, Phys. Rev. Lett. **110**, 025902 (2013).
[18] M. Trigo, A. Bruchhausen, A. Fainstein, B. Jusserand, and V. Thierry-Mieg, Phys. Rev. Lett. **89**, 227402 (2002).
[19] D. Schneider, F. Liaqat, O. El Abouti, W. Tremel, H.-J. Butt, B. Djafari-Rouhani, and G. Fytas, Phys. Rev. Lett. **111**, 164301 (2013).
[20] N.-W. Pu and J. Bokor, Phys. Rev. Lett. **91**, 076101 (2003).
[21] N. Lanzillotti-Kimura, A. Fainstein, B. Perrin, B. Jusserand, A. Soukiassian, X. Xi, and D. Schlom, Phys. Rev. Lett. **104**, 187402 (2010).
[22] R. Beardsley, A. Akimov, M. Henini, and A. Kent, Phys. Rev. Lett. **104**, 085501 (2010).
[23] B. Liang, X. Guo, J. Tu, D. Zhang, and J. Cheng, Nat. Mater. **9**, 989 (2010).
[24] M. Eichenfield, J. Chan, R. M. Camacho, K. J. Vahala, and O. Painter, Nature **462**, 78 (2009).
[25] A. H. Safavi-Naeini, and O. Painter, Opt. Express **18**, 14926 (2010).
[26] M. Kataoka, M. Astley, A. Thorn, D. Oi, C. Barnes, C. Ford, D. Anderson, G. Jones, I. Farrer, and D. Ritchie, Phys. Rev. Lett. **102**, 156801 (2009).
[27] V. Miseikis, J. Cunningham, K. Saeed, R. O'Rorke, and A. Davies, Appl. Phys. Lett. **100**, 133105 (2012).
[28] J. Schiefele, J. Pedrós, F. Sols, F. Calle, and F. Guinea, Phys. Rev. Lett. **111**, 237405 (2013).
[29] P. Thalmeier, B. Dóra, and K. Ziegler, Phys. Rev. B **81**, 041409 (2010).
[30] Y. Tanaka and S. Tamura, Phys. Rev. B **58**, 7958 (1998).
[31] S. Benchabane, A. Khelif, J.-Y. Rauch, L. Robert, and V. Laude, Phys. Rev. E **73**, 065601 (2006).
[32] D. Yudistira, Y. Pennec, B. D. Rouhani, S. Dupont, and V. Laude, Appl. Phys. Lett. **100**, 061912 (2012).
[33] Y.-Z. Wang, F.-M. Li, W.-H. Huang, and Y.-S. Wang, J. Phys. Condens. Matter **19**, 496204 (2007).
[34] K. Huang, Dynamical Theory of Crystal Lattices, Oxford University Press, Incorporated (1954).
[35] C. Huang and Y. Zhu, Phys. Rev. Lett. **94**, 117401 (2005).
[36] J. D. Caldwell, L. Lindsay, V. Giannini, I. Vurgaftman, T. L. Reinecke, S. A. Maier, and O. J. Glembocki, Nanophotonics **4**, 44 (2015).
[37] D. Yudistira, A. Boes, D. Janner, V. Pruneri, J. Friend, and A. Mitchell, J. Appl. Phys. **114**, 054904 (2013).
[38] D. Yudistira, A. Boes, B. Djafari-Rouhani, Y. Pennec, L. Yeo, A. Mitchell, and J. Friend, Phys. Rev. Lett. **113**, 215503 (2014).
[39] D. Yudistira, D. Janner, S. Benchabane, and V. Pruneri, Opt. Lett. **34**, 3205 (2009).
[40] D. Yudistira, S. Benchabane, D. Janner, and V. Pruneri, Appl. Phys. Lett. **98**, 233504 (2011).
[41] D. Janner, D. Tulli, M. Jofre, D. Yudistira, S. Balsamo, M. Belmonte, and V. Pruneri, IEEE J. Sel. Top. Quantum Electron. **19**, 3400610 (2013).
[42] D. Yudistira, A. Boes, A. R. Rezk, L. Y. Yeo, J. R. Friend, and A. Mitchell, Adv. Mater. Interfaces **1** (2014).
[43] D. Morgan, Surface Acoustic Wave Filters, Second Edition: With Applications to Electronic Communications and Signal Processing, Academic Press (2007).